Effect of Molecular Rigidity on Micelle Formation in Amphiphilic Solution

Susumu FUJIWARA, Takashi ITOH, Masato HASHIMOTO, Hiroaki NAKAMURA[1)] and Yuichi TAMURA[2)]

Kyoto Institute of Technology, Matsugasaki, Sakyo-ku, Kyoto 606-8585, Japan
[1)]*National Institute for Fusion Science, 322-6 Oroshi-cho, Toki 509-5292, Japan*
[2)]*Konan University, 8-9-1 Okamoto, Higashinada-ku, Kobe 658-8501, Japan*

(Received 8 December 2009 / Accepted 5 February 2010)

Micelle formation in an amphiphilic solution is investigated by a molecular dynamics simulation of coarse-grained semiflexible amphiphilic molecules with explicit solvent molecules. Our simulations show that the micellar shape changes from a cylinder to a disc as the intensity of the molecular rigidity increases. We find that the radius of gyration of the cylindrical micelle is larger than that of the disc-shaped micelle for small molecular rigidity, although the radius of gyration is almost steady even during the transition between a cylinder and a disc for large molecular rigidity. This indicates that a cylindrical micelle formed at small molecular rigidity is more anisotropic than the one obtained at large molecular rigidity. We also ascertained that a cylindrical micelle and a disc-shaped micelle coexist dynamically over a certain molecular rigidity range.

Keywords: molecular dynamics simulation, molecular rigidity, micelle formation, micellar shape, amphiphilic solution

DOI: 10.1585/pfr.5.S2114

1. Introduction

The spontaneous formation of structures in plasmas has been intensively studied to improve plasma confinement. Such creation of order, or self-organization, is a universal characteristic of nonequilibrium and nonlinear systems interacting with the environment. To explore universal self-organizing properties in nature, we investigate self-organization in other systems such as polymeric systems [1–6] and amphiphilic systems [7–9].

Amphiphilic molecules, such as lipids and surfactants, contain both a hydrophilic part and a hydrophobic part. In aqueous solvents, these molecules self-assemble spontaneously into various structures such as micelles, bilayer membranes, and bicontinuous cubic structures [10–12]. Self-assembly of amphiphilic molecules plays an important role in several biological and industrial processes.

Several computer simulations have been performed to examine the effect of molecular rigidity on structure formation in polymers. Miura *et al.* studied the effect of rigidity on the crystallization processes of polymer melts by a molecular dynamics (MD) simulation [13]. Computer simulations of a single semiflexible homopolymer [14] and a single flexible-semiflexible block copolymer [15] have been performed to investigate the folding transition. However, few simulation studies have been conducted systematically to examine the effect of molecular rigidity on micelle formation in an amphiphilic solution.

The purpose of this study is to clarify the molecular mechanism of micelle formation in an amphiphilic solution. Our particular concern is to investigate the effect of molecular rigidity on micelle formation. To investigate this in the amphiphilic solution at the molecular level, we perform MD simulations of coarse-grained semiflexible amphiphilic molecules with explicit solvent molecules and analyze the micelle formation process.

2. Simulation Model and Method

The computational model is similar to that used in the previous study [7–9], which is based on the model of Goetz *et al.* [16]. An amphiphilic molecule is a semiflexible chain consisting of one hydrophilic particle and three hydrophobic particles. A solvent molecule is modeled as a hydrophilic particle. Particles interact via the nonbonded and bonded potentials.

For nonbonded potentials, the interaction between a hydrophilic particle and a hydrophobic particle is modeled by a repulsive soft core potential

$$U_{\mathrm{SC}}(r) = 4\varepsilon_{\mathrm{SC}}\left(\frac{\sigma_{\mathrm{SC}}}{r}\right)^9. \tag{1}$$

The interaction between a hydrophilic head particle and a solvent particle is modeled by the Lennard-Jones potential

$$U_{\mathrm{LJ-hs}}(r) = 4\varepsilon_{\mathrm{hs}}\left[\left(\frac{\sigma}{r}\right)^{12} - \left(\frac{\sigma}{r}\right)^{6}\right], \tag{2}$$

and all other interactions are modeled by the Lennard-Jones potential

author's e-mail: fujiwara@kit.ac.jp

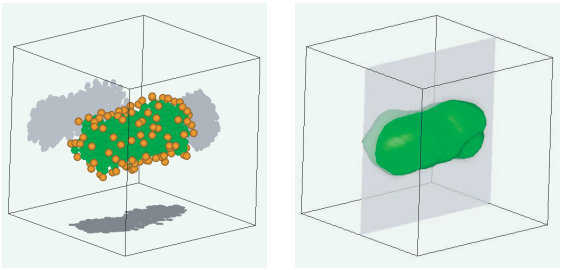

(a) (b)

Fig. 1 (a) Snapshot of a cylindrical micelle and (b) an isosurface of tail particles formed by amphiphilic molecules at $t^* = 4800$ for $k_3^* = 4.0$ and $(\varepsilon_{SC}^*, \varepsilon_{hs}^*) = (1.0, 2.0)$. In (a), gray shadows of the micelle projected on three planes are also depicted to illustrate its shape. Orange and green particles denote hydrophilic head particles and hydrophobic tail particles, respectively. Note that, for clarity, solvent molecules are not displayed.

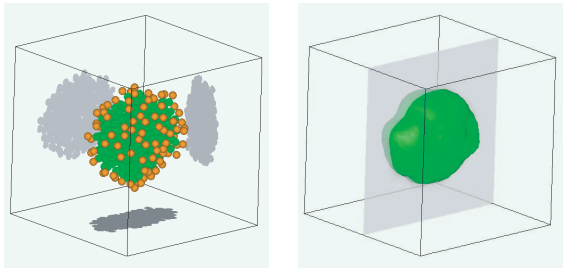

(a) (b)

Fig. 2 (a) Snapshot of a disc-shaped micelle and (b) an isosurface of tail particles formed by amphiphilic molecules at $t^* = 5000$ for $k_3^* = 16.0$ and $(\varepsilon_{SC}^*, \varepsilon_{hs}^*) = (1.0, 2.0)$. In (a), gray shadows of the micelle projected on three planes are also depicted to illustrate its shape. Orange and green particles denote hydrophilic head particles and hydrophobic tail particles, respectively. Note that, for clarity, solvent molecules are not displayed.

$$U_{LJ}(r) = 4\varepsilon\left[\left(\frac{\sigma}{r}\right)^{12} - \left(\frac{\sigma}{r}\right)^{6}\right]. \quad (3)$$

Here, r is the interparticle distance, ε_{SC} is an interaction parameter representing the intensity of the hydrophobic interaction, and ε_{hs} represents the intensity of the hydrophilic interaction. The parameter σ_{SC} is set to $\sigma_{SC} = 1.05\sigma$, as in Ref. [16]. To avoid discontinuities in both the potential energy and the force due to the potential energy cutoff, we use the shifted force variant of these nonbonded potentials

$$V_X(r) = U_X(r) - U_X(r_c) - \left.\frac{\partial U_X}{\partial r}\right|_{r=r_c}(r - r_c), \quad (4)$$

where X = SC, LJ-hs, or LJ, and r_c is the cutoff distance, which is set to $r_c = 3.0\sigma$ here.

As bonded potentials, we consider a bond-stretching potential

$$U_2(d_i) = k_2(d_i - \sigma)^2, \quad (5)$$

where k_2 is the bond-stretching modulus and d_i is the bond length between two neighboring particles along the amphiphilic molecule and a bond-bending potential

$$U_3(\phi_i) = k_3(1 - \cos\phi_i), \quad (6)$$

where k_3 is the bending modulus of the semiflexible amphiphiles and ϕ_i is the tilt angle between two neighboring bonds. The parameter k_2 is set to $k_2 = 5000\varepsilon\sigma^{-2}$, as in Ref. [16]. The molecular rigidity is controlled by the bending modulus k_3. In the following sections, we represent dimensionless quantities by an asterisk, e.g., number density $\rho^* = \rho\sigma^3$, time $t^* = t\sqrt{\varepsilon/m\sigma^2}$, and temperature $T^* = k_B T/\varepsilon$, where k_B is the Boltzmann constant.

The equations of motion for all particles are solved numerically by using the velocity Verlet algorithm at constant temperature with a time step of $\Delta t^* = 0.0005$, and the temperature is controlled at every 10 time steps by ad hoc velocity scaling [17]. We apply periodic boundary conditions, and the number density is set to $\rho^* = 0.75$.

First, we prepare an isolated micelle of 120 flexible amphiphilic molecules with $k_3^* = 0.0$ in solution at $T^* = 1.3$ for various values of the interaction parameters ε_{SC}^* and ε_{hs}^* ($1.0 \le \varepsilon_{SC}^*, \varepsilon_{hs}^* \le 3.0$). The number of solvent molecules is 7520, which yields an amphiphilic concentration of 0.06. The bending modulus k_3^* is then changed to various values ($k_3^* = 1.0, 2.0, 4.0, 8.0, 16.0$) and MD simulations of $t^* = 5.0 \times 10^3$ (1.0×10^7 time steps) are carried out for each simulation run. In this paper, we focus on the results for $\varepsilon_{SC}^* = 1.0$.

3. Simulation Results and Discussion

3.1 Micellar shape

In Figs. 1 and 2, we show snapshots of micelles formed by amphiphilic molecules at $(\varepsilon_{SC}^*, \varepsilon_{hs}^*) = (1.0, 2.0)$ for $k_3^* = 4.0$ and $k_3^* = 16.0$, respectively. Gray shadows of the amphiphilic molecules projected on three planes and an isosurface of the tail particles, which is calculated by Gaussian splatting techniques, are depicted in (a) and (b), respectively, to show the micellar shape clearly. Figures 1 and 2 show that the micellar structure formed at $k_3^* = 4.0$ is cylindrical and that at $k_3^* = 16.0$ is disc-shaped. Our simulations indicate that the micellar shape changes from a cylinder to a disc as the intensity of the molecular rigidity, k_3^*, increases.

3.2 Potential energy, radius of gyration, and micellar shape distribution

In this subsection, we examine the potential energy E_{pot}^*, the radius of gyration of the micelle R_g^*, and the micellar shape distribution in order to quantitatively investigate how the micellar shape changes with the molecular rigidity. As in our previous papers [8, 9], we use the orientational order parameters as indices to characterize the micellar shape. We introduce a coordinate system that uses the three principal axes of inertia of the micelle. The origin is located at the center-of-mass position of the micelle,

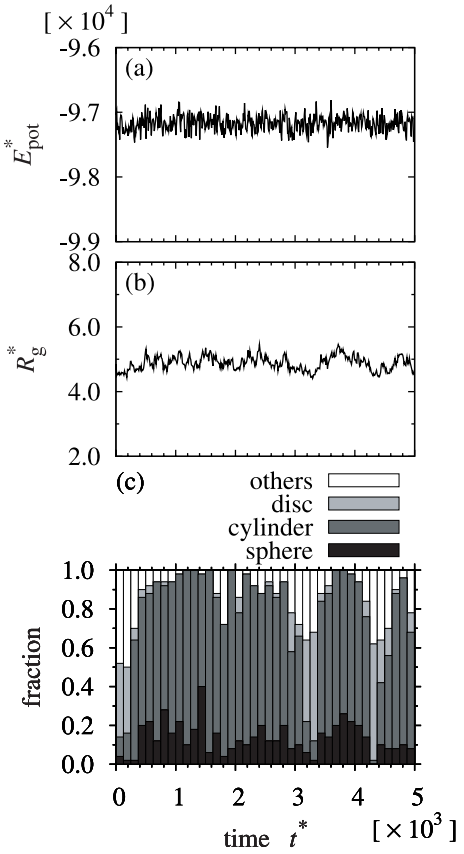

Fig. 3 Time evolution of (a) the total potential energy $E^*_{\rm pot}$, (b) the radius of gyration $R^*_{\rm g}$ of the micelle, and (c) the fraction of various micellar shapes at $k^*_3 = 4.0$ and $(\varepsilon^*_{\rm SC}, \varepsilon^*_{\rm hs}) = (1.0, 2.0)$.

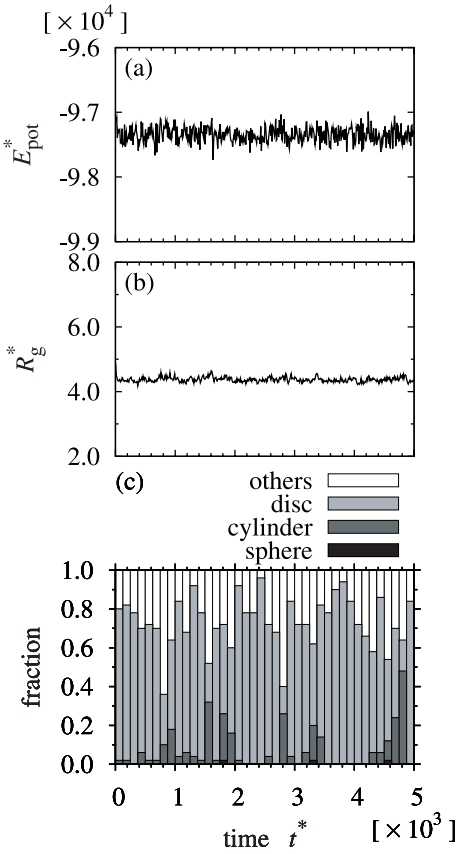

Fig. 4 Time evolution of (a) the total potential energy $E^*_{\rm pot}$, (b) the radius of gyration $R^*_{\rm g}$ of the micelle, and (c) the fraction of various micellar shapes at $k^*_3 = 16.0$ and $(\varepsilon^*_{\rm SC}, \varepsilon^*_{\rm hs}) = (1.0, 2.0)$.

the x-axis is the principal axis with the largest moment of inertia, and the z-axis is the principal axis with the smallest moment of inertia. The orientational order parameters p_x, p_y, and p_z are defined by

$$p_i = \left\langle \frac{3\cos^2\theta_i - 1}{2} \right\rangle \quad (i = x, y, z), \tag{7}$$

where θ_i is the angle between the end-to-end vector of an amphiphilic molecule and the i-axis ($i = x, y, z$), and $\langle \cdots \rangle$ denotes the average over of all amphiphilic molecules. Note that the average is taken for the amphiphilic molecules in the vicinity of the center-of-mass position of the micelle, that is, those in the region $-\Delta r < x, y, z < \Delta r$. We set $\Delta r = 2.5\sigma$ in the calculation of p_i. Ideally, the orientational order parameters take the following values: $(p_x, p_y, p_z) = (1, -0.5, -0.5)$ for a disc: $(p_x, p_y, p_z) = (0, 0, -0.5)$ for a cylinder: and $(p_x, p_y, p_z) = (0, 0, 0)$ for a sphere. Detailed analysis of the distribution functions of these orientational order parameters showed that, in practice, three types of micellar shapes are clearly distinguishable by the orientational order parameters: $0.5 < p_x < 1.0$ and $-0.5 < p_y, p_z < -0.25$ for a disc-shaped micelle: $-0.25 < p_x, p_y < 0.5$ and $-0.5 < p_z < -0.25$ for a cylindrical micelle: and $-0.25 < p_x, p_y, p_z < 0.5$ for a spherical micelle [8, 9]. We calculate the fractions of the micellar shapes on the basis of these orientational order parameters.

Figures 3 and 4 show the time dependence of the total potential energy $E^*_{\rm pot}$, the radius of gyration of the micelle $R^*_{\rm g}$, and the fraction of various micellar shapes at $k^*_3 = 4.0$ and $k^*_3 = 16.0$, respectively. The following characteristic features are identified. (1) The dominant micellar shape at $k^*_3 = 4.0$ is a cylinder (Fig. 3 (c)), and that at $k^*_3 = 16.0$ is a disc (Fig. 4 (c)), and the micellar shape alternates between a cylinder and a disc several times, e.g., at $t^* \approx 3300$ and 4300 in Fig. 3 (c) and at $t^* \approx 4800$ in Fig. 4 (c). Such an alternating behavior can be a precursor to the dynamic coexistence discussed below (section 3.3). (2) The potential energy remains almost constant even during the transition between a cylinder and a disc (Figs. 3 (a) and 4 (a)). (3) The radius of gyration of the cylindrical micelle becomes larger than that of the disc-shaped micelle at $k^*_3 = 4.0$ (Fig. 3 (b)), whereas the radius of gyration is almost steady even during the transition between a cylinder and a disc at $k^*_3 = 16.0$ (Fig. 4 (b)). This indicates that the cylindrical micelle formed at $k^*_3 = 4.0$ is more anisotropic than that obtained at $k^*_3 = 16.0$.

3.3 Dynamic coexistence of micellar shapes

Here, we study the dynamic coexistence of a cylindri-

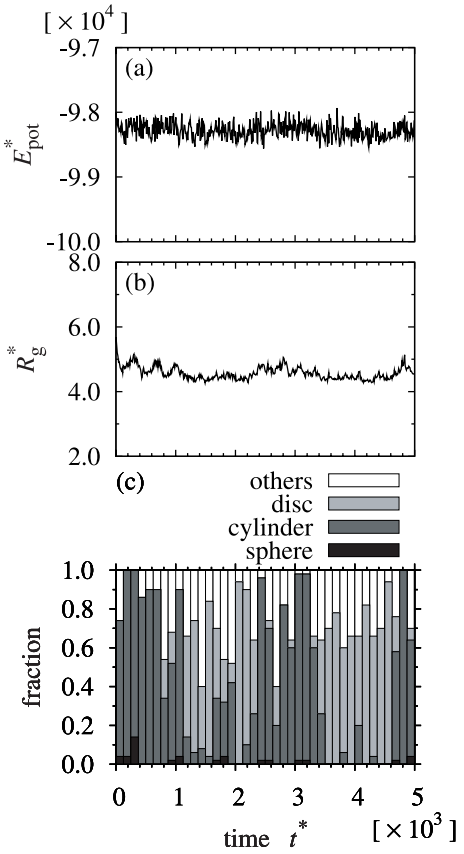

Fig. 5 Time evolution of (a) the total potential energy $E^*_{\rm pot}$, (b) the radius of gyration $R^*_{\rm g}$ of the micelle, and (c) the fraction of various micellar shapes at $k^*_3 = 16.0$ and $(\varepsilon^*_{\rm SC}, \varepsilon^*_{\rm hs}) = (1.0, 2.5)$.

cal micelle and a disc-shaped micelle observed at $k^*_3 = 16.0$ and $(\varepsilon^*_{\rm SC}, \varepsilon^*_{\rm hs}) = (1.0, 2.5)$. In Fig. 5, we show the time dependence of the total potential energy $E^*_{\rm pot}$, the radius of gyration of the micelle $R^*_{\rm g}$, and the fraction of various micellar shapes. Figure 5 (c) indicates that the dominant micellar shape alternates between a cylinder and a disc. Both the potential energy and the radius of gyration for the cylindrical micelle become larger than those for the disc-shaped micelle, which means that the disc-shaped micelle is more stable and isotropic than the cylindrical micelle.

4. Conclusion

We have obtained the following new results by performing MD simulations of coarse-grained semiflexible amphiphilic molecules with explicit solvent molecules. (1) As the intensity of the molecular rigidity k^*_3 increases, the micellar shape changes from a cylinder to a disc. (2) The radius of gyration of a cylindrical micelle is larger than that of a disc-shaped micelle for small k^*_3, whereas the radius of gyration becomes almost constant even during the transition between a cylinder and a disc for large k^*_3. (3) The dynamic coexistence of a cylindrical micelle and a disc-shaped micelle is observed over a certain molecular rigidity range. Both the potential energy and radius of gyration of the cylindrical micelle become larger than those of the disc-shaped micelle.

The second result indicates that the cylindrical micelle formed at small k^*_3 is more anisotropic than that obtained at large k^*_3. The third observation suggests that the disc-shaped micelle is more stable and isotropic than the cylindrical micelle.

Dynamic coexistence is observed not only in amphiphilic systems but also in polymeric systems. In polymeric systems, dynamic coexistence of the orientationally ordered state and the randomly oriented state is observed at a certain temperature [5].

As our future work, we will study the molecular mobility and micellar shape change in semiflexible amphiphilic solutions.

Acknowledgment

This study was partially supported by a Grants-in-Aid (No. 19031019) from the Ministry of Education, Culture, Sports, Science and Technology, Japan. This study was performed with the support and under the auspices of the NIFS Collaborative Research Program (NIFS07KDAN002).

[1] S. Fujiwara and T. Sato, J. Chem. Phys. **107**, 613 (1997).
[2] S. Fujiwara and T. Sato, J. Chem. Phys. **114**, 6455 (2001).
[3] S. Fujiwara and T. Sato, Phys. Rev. Lett. **80**, 991 (1998).
[4] S. Fujiwara and T. Sato, J. Chem. Phys. **110**, 9757 (1999).
[5] S. Fujiwara and T. Sato, Comput. Phys. Commun. **142**, 123 (2001).
[6] S. Fujiwara, M. Hashimoto, T. Itoh and H. Nakamura, J. Phys. Soc. Jpn. **75**, 024605 (2006).
[7] S. Fujiwara, M. Hashimoto and T. Itoh, J. Plasma Phys. **72**, 1011 (2006).
[8] S. Fujiwara, T. Itoh, M. Hashimoto and Y. Tamura, Mol. Simul. **33**, 115 (2007).
[9] S. Fujiwara, T. Itoh, M. Hashimoto and R. Horiuchi, J. Chem. Phys. **130**, 144901 (2009).
[10] J. N. Israelachvili, *Intermolecular and Surface Forces* (Academic Press, London, 1992) 2nd ed.
[11] *Micelles, Membranes, Microemulsions, and Monolayers*, edited by W. M. Gelbart, A. Ben-Shaul and D. Roux (Springer-Verlag, New York, 1994), pp. 1–104.
[12] I. W. Hamley, *Introduction to Soft Matter* (J. Wiley, Chichester, 2000).
[13] T. Miura, R. Kishi, M. Mikami and Y. Tanabe, Phys. Rev. E **63**, 061807 (2001).
[14] T. Sakaue and K. Yoshikawa, J. Chem. Phys. **117**, 6323 (2002).
[15] N. Yoshinaga and K. Yoshikawa, J. Chem. Phys. **127**, 044902 (2007).
[16] R. Goetz and R. Lipowsky, J. Chem. Phys. **108**, 7397 (1998).
[17] M. P. Allen and D. J. Tildesley, *Computer Simulation of Liquids* (Clarendon, Oxford, 1987).